Journal of Power Sources 190 (2009) 408–416

Contents lists available at ScienceDirect

Journal of Power Sources

journal homepage: www.elsevier.com/locate/jpowsour

High efficiency process for the production of pure oxygen based on solid oxide fuel cell–solid oxide electrolyzer technology

Paolo Iora [a,*], Paolo Chiesa [b]

[a] Università degli Studi di Brescia, Dipartimento di Ingegneria Meccanica e Industriale, Via Branze, 38 – 25123 Brescia, Italy
[b] Politecnico di Milano, Dipartimento di Energia, Piazza Leonardo da Vinci, 32 – 20133 Milano, Italy

ARTICLE INFO

Article history:
Received 19 September 2008
Received in revised form 18 December 2008
Accepted 18 January 2009
Available online 25 February 2009

Keywords:
Solid oxide fuel cell
Solid oxide electrolyzer
Oxygen production
Planar cell

ABSTRACT

This paper presents a novel system for production of pure oxygen based on the integration of a solid oxide fuel cell (SOFC) and a solid oxide electrolyzer (SOEC). In the proposed arrangement, the SOFC provides electricity, heat and H_2O in vapour phase to the SOEC which carries out the inverse reactions of the SOFC, that is the separation of H_2O into H_2 (used as a fuel for the SOFC) and O_2 (representing the yield of the system). Simulations carried out in different operating conditions show that when the integrated SOFC–SOEC device runs at low current densities (less than 1000 A m^{-2}), pure oxygen can be generated with an electric consumption comparable to mid-size cryogenic air separation units, and significantly lower than small scale systems based on the PSA technology.

1. Introduction

Oxygen, as a pure component or in high concentration mixtures, is used in many field of the industry as well as in medical treatments [1]. Usually it is obtained from air by means of cryogenic and non-cryogenic air separation technologies [2,3]. The cryogenic systems can fractionate air in a distillation process carried out at temperature of about −160 °C by exploiting the different liquefaction temperatures of O_2 and N_2. They may deliver large oxygen flow rate (over 3000 ton_{O_2} per day in a single line) with purity close to 100% and, among all the air separation technologies, they are the most cost-effective and the most efficient in terms of energy consumption per unit of product, when high flow rates of oxygen are requested. Specific consumption for "tonnage" plants can reach 0.2 kW h per kg of 95% purity oxygen [2,4]. On the other hand, for production lower than about 50 ton_{O_2} day^{-1}, alternative technologies become more economically advantageous [5]. This is because small size cryogenic plants have less efficient compressors and a higher thermal input to the cold-box. As a matter of fact in a small scale plant the specific consumption can be 50% higher than that of a large production unit [6].

Non-cryogenic systems are most commonly employed at the lower end of the output rate scale and when high purity oxygen is not needed (typically less than 94%). They are based on PSA (pressure swing adsorption), VSA (vacuum swing adsorption) technologies, or hybrid solutions between the former ones, which exploit the greater affinity for N_2 than for O_2 of specific adsorbent materials such as the zeolites. Such devices show energy consumption in the range 0.7–1 kW h $kg_{O_2}{}^{-1}$ for product rates from 800 to 70 kg_{O_2} day^{-1}. [7,8]. Besides, other systems based on chemical processes and membrane separation technologies are under testing, but presently do not commercially compete with the processes mentioned so far.

In principle oxygen can also be obtained through the electrolysis of water (H_2O); however the high electrical consumption of this process makes this option not competitive with the state-of-the-art technologies. A possible solution capable to improve the efficiency of oxygen production via electrolysis would imply using H_2 (the co-product of the water electrolysis) as a fuel to generate the electricity required by the electrolysis itself. This process can be carried out by the integration of an engine with a common water-electrolyzer, as it is reported in Fig. 1. The operating principles are the following:

- the water-electrolyzer allows the separation of H_2O into the two elements, hydrogen and oxygen. The first is used as a fuel for the engine, while oxygen is stored in a tank.
- the engine uses hydrogen given by the water-electrolyzer as a fuel and ambient air as oxidizer, producing part of the electricity consumed by the water-electrolyzer.

However the amount of H_2 generated through the electrolysis is less than that required by the engine to produce the electricity necessary for water dissociation. This is due to the losses in the

* Corresponding author. Tel.: +39 030 3715498; fax: +39 030 3702448.
E-mail addresses: paolo.iora@ing.unibs.it (P. Iora), paolo.chiesa@polimi.it (P. Chiesa).

0378-7753/$ – see front matter © 2009 Elsevier B.V. All rights reserved.
doi:10.1016/j.jpowsour.2009.01.045

Nomenclature

A	area (m^2)
BP	SOEC anode side back pressure (bar)
E	specific work ($J\,mol^{-1}$)
E^0	standard potential (V)
F	Faraday's constant: 96487 $C\,mol^{-1}$
ΔG	Gibbs free energy change of the reaction ($J\,mol_{H_2}{}^{-1}$)
h	static enthalpy (J)
h^0	total enthalpy (J)
ΔH	enthalpy change of the reaction ($J\,mol_{H_2}{}^{-1}$)
I	current (A)
L	work (J)
N	number of moles
$\dot{N}$	mole flow rate ($mol\,s^{-1}$)
p	pressure (bar)
R	universal gas constant: 8.314 $J\,mol^{-1}\,K^{-1}$
SOEC	solid oxide electrolyzer
SOFC	solid oxide fuel cell
ΔS	entropy change of the reaction ($J\,mol_{H_2}{}^{-1}\,K^{-1}$)
T	temperature (K)
v	velocity ($m\,s^{-1}$)
V	cell voltage (V); volume (m^3)
W	electric power (W)
X_i	molar fraction of specie i (−)

Subscripts

aux	auxiliary
el	electric
FIN	final
is	isentropic
re	real
rev	reversible
spec	specific
tot	total

components and to the fact that the energy required for the separation of a mixture is greater than zero even in an ideal, reversible process. Therefore in order to allow a continuous operation of the process as shown in Fig. 1, it is necessary to provide auxiliary energy, either as electricity to the electrolyzer (shown in the figure as $W_{el,aux}$) or as a fuel integration for the engine.

Nevertheless, the resulting energy consumption is still too high to compete with the traditional air separation technologies. This is mainly due to the relatively low efficiency of the electrolyzer (70–75%, calculated as the ratio between the LHV-flow rate associated to the H_2 output and the electric power consumption) and of the engine (35–40%).

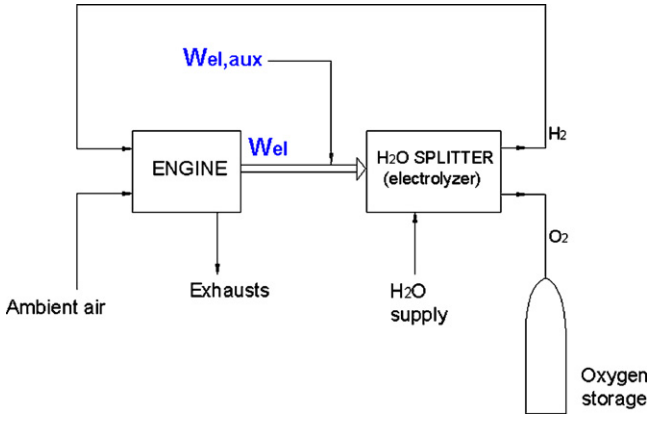

Fig. 1. Conceptual scheme of the process for oxygen production via electrolysis.

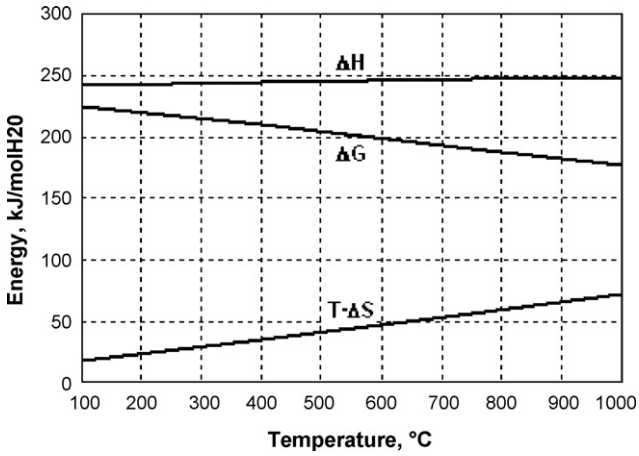

Fig. 2. Thermal ($T\Delta S$), electrical (ΔG) and total (ΔH) energy consumption for the steam electrolysis as a function of temperature.

As a matter of fact, typical electrolyzers available on the market, operate the dissociation of H_2O in liquid phase (normally at ambient conditions): in this case the variation of the Gibbs free energy (ΔG) for the reaction $H_2O \rightarrow H_2 + 1/2O_2$ – which represents the minimum quantity of electrical energy required in the reaction – is 237 $kJ\,mol_{H_2O}{}^{-1}$. It is worth to note that the value of ΔG lowers to 228 $kJ\,mol_{H_2O}{}^{-1}$ if the molecule of water is in vapour phase (at ambient conditions) and decreases as temperature is raised (for instance it becomes 190 $kJ\,mol_{H_2O}{}^{-1}$ at 750 °C). Therefore, from a thermodynamic point of view it is advantageous to carry out a steam-electrolysis at high temperature, although this imply, on the other hand, a progressive increase of the heat required in the reaction. Fig. 2 explains this point: $T\Delta S$ and ΔG, respectively represent the thermal and electrical energies consumed in the reaction, while ΔH corresponds to the total energy consumption, in the absence of irreversible losses. Although ΔH remains approximately constant, ΔG tends to decrease while $T\Delta S$ tends to increase as the temperature is raised. This means that with the increase of temperature, it is possible to replace part of the electrical energy with heat, which is, according to the second law of thermodynamics, a lower grade energy form.

As a consequence, a significant improvement of the system shown in Fig. 1 can be achieved if the cogenerated heat produced by the engine is used together with the generated electricity in a steam-electrolyzer operating at high temperature.

2. Integrated SOFC–SOEC system

The conceptual scheme described in the previous paragraph finds a very efficient application in an integrated SOFC–SOEC system. The SOFC (solid oxides fuel cell) [9] is a high temperature (>650 °C) fuel cell that produces electric and thermal energy and steam from hydrogen and oxygen. The SOEC (solid oxide electrolyzer) [10] is an electrolyzer that carries out inverse process of a SOFC. In Fig. 3 the working principles of the two components are presented. In this configuration SOFC and SOEC replace the engine and the H_2O splitter in the scheme reported in Fig. 1. A detailed description of the system layout and the related energy balances will be reported in Section 2.2.

2.1. Thermodynamic principles

As it will be better explained later, the energy consumption of the SOFC–SOEC system is due to the difference between the

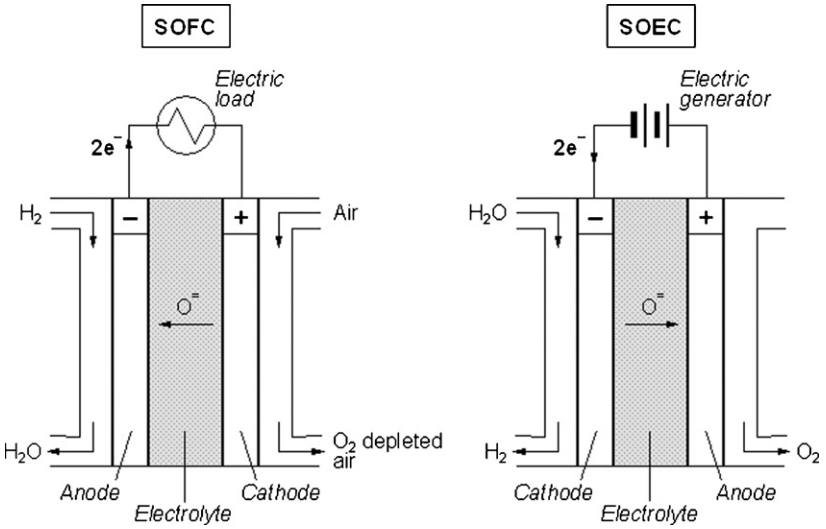

Fig. 3. Working principles of solid oxides fuel cells (SOFC) and solid oxides electrolyzer (SOEC).

operating voltage of SOFC and SOEC. It is therefore helpful to evaluate these quantities starting from the ideal conditions. To this purpose, a conceptual scheme showing an integrated SOFC–SOEC system is reported in Fig. 4. In this configuration a H_2–H_2O mixture is continuously recirculated between the anode of the SOFC (where H_2 is consumed and H_2O is produced) and the cathode of the SOEC (where the H_2O produced by the SOFC is reconverted into H_2). The SOFC cathode is fed with ambient air where oxygen is considered at a partial pressure of 0.21 atm. The result of the process is the production of O_2 at SOEC anode. By assuming that the molar flow rate of air fed at the SOFC cathode and of the recirculated H_2–H_2O stream is significantly higher than the one of the oxygen produced, it follows that the composition of the two former streams can be considered approximately constant through the cells. It is also assumed that the system operates at constant temperature T which is uniform over the SOFC and SOEC.

Under these assumptions the reversible potential can be directly deduced from the Nernst equation for SOFC and SOEC:

$$V_{\text{rev}}^{\text{SOEC}} = E^0 + \frac{RT}{2F} \ln \left(\frac{X_{\text{H}_2}^{\text{SOEC}} \sqrt{p_{\text{O}_2}^{\text{SOEC}}}}{X_{\text{H}_2\text{O}}^{\text{SOEC}}} \right) \tag{1}$$

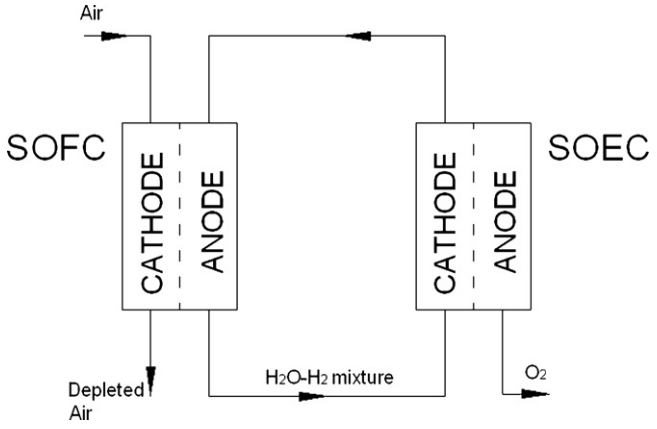

Fig. 4. Conceptual layout of an integrated SOFC–SOEC system for pure oxygen production.

$$V_{\text{rev}}^{\text{SOFC}} = E^0 + \frac{RT}{2F} \ln \left(\frac{X_{\text{H}_2}^{\text{SOFC}} \sqrt{p_{\text{O}_2}^{\text{SOFC}}}}{X_{\text{H}_2\text{O}}^{\text{SOFC}}} \right) \tag{2}$$

where E^0 is the temperature dependent standard potential, calculated at the standard pressure of 1 atm. Accordingly, p_{O_2} is the partial pressure of the oxygen expressed in atm.

Subtracting (2) from (1) we obtain the SOEC–SOFC reversible voltage difference:

$$V_{\text{rev}}^{\text{SOEC}} - V_{\text{rev}}^{\text{SOFC}} = \frac{RT}{4F} \ln \left(\frac{p_{\text{O}_2}^{\text{SOEC}}}{p_{\text{O}_2}^{\text{SOFC}}} \right) \tag{3}$$

If the current I circulates in the cells, the resulting power consumption of the ideal SOFC–SOEC system will be:

$$W_{\text{rev}} = I \left(V_{\text{rev}}^{\text{SOEC}} - V_{\text{rev}}^{\text{SOFC}} \right) = I \frac{RT}{4F} \ln \left(\frac{p_{\text{O}_2}^{\text{SOEC}}}{p_{\text{O}_2}^{\text{SOFC}}} \right) \tag{4}$$

Since the current I can be expressed as a function of the mole flow rate of the O_2 output as:

$$I = \dot{N}_{\text{O}_2} 4F \tag{5}$$

and by combining Eqs. (4) and (5) we obtain the specific energy required for oxygen production:

$$E_{\text{rev}} = \frac{W_{\text{rev}}}{\dot{N}_{\text{O}_2}} = \frac{I \left(V_{\text{rev}}^{\text{SOEC}} - V_{\text{rev}}^{\text{SOFC}} \right)}{\dot{N}_{\text{O}_2}} = \frac{RT}{4F} \ln \left(\frac{p_{\text{O}_2}^{\text{SOEC}}}{p_{\text{O}_2}^{\text{SOFC}}} \right) \tag{6}$$

which is equivalent to the ideal work required to separate and make available at pressure $p_{O_2}^{SOEC}$ the oxygen contained in the ambient air at the partial pressure $p_{O_2}^{SOFC}$ (assumed as 0.21 bar) in a isothermal process carried out at temperature T (see Appendix A).

With reference to the value of $p_{O_2}^{SOEC}$, three cases are worth to be considered:

(a) $p_{O_2}^{SOEC} > p_{O_2}^{SOFC}$

This is the case where oxygen is produced by the SOEC for instance at ambient pressure. This solution brings about the advantage of avoiding any further O_2 compression; on the other hand the power absorbed by the SOFC–SOEC is grater than zero

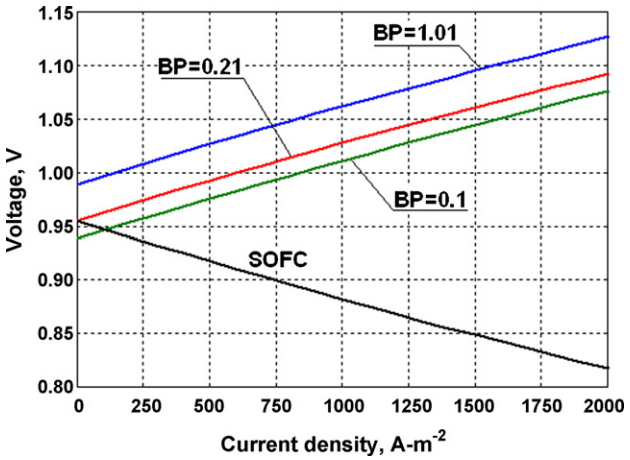

Fig. 5. Examples of voltage–current curves for SOFC and SOEC operating at different pressures.

and proportional to the operating temperature according to Eq. (6).

(b) $p_{O_2}^{SOEC} = p_{O_2}^{SOFC}$

The oxygen produced by the SOEC has the same pressure of the oxygen in the air and ideally no power is supplied to the SOFC–SOEC system. Power is required subsequently to bring the oxygen to ambient pressure. This solution is more efficient than case (a) because the compression process can be carried out after cooling O_2 at ambient temperature thus reducing the power required according to Eq. (6).

(c) $p_{O_2}^{SOEC} < p_{O_2}^{SOFC}$

The SOFC–SOEC system generates power which in an ideal case is equal to the power that can be obtained in an ideal isothermal expansion of O_2 from $p_{O_2}^{SOFC}$ (0.21 bar in this case) to $p_{O_2}^{SOEC}$. This is possible only if an equal amount of heat is provided to the SOEC in order to equilibrate the energy balance of the SOFC–SOEC system.

Aiming to better focus these aspects, Fig. 5 shows in the V–I plane a typical curve of a SOFC (operating at ambient pressure) together with three curves of SOECs characterized by different anode side back pressures. Curve SOEC BP = 1.01 refers to the case where oxygen is produced at ambient pressure. It can be seen that at open circuit ($I = 0$) V_{rev}^{SOEC} is higher than V_{rev}^{SOFC}; in this condition the difference of the two voltages can be calculated according to Eq. (3) and yields about 0.034 V (at $T = 750$ K). Curve BP = 0.21 and BP = 0.1 refer to the cases where back pressure is $p = 0.21$ bar and $p = 0.1$ bar respectively. For $I = 0$ curves SOFC and SOEC BP = 0.21 have the same reversible potential, while a negative difference $V_{rev}^{SOEC} - V_{rev}^{SOFC}$ results for the case BP = 0.1. On real operating conditions, when the device runs at $I > 0$, activation, ohmic, and concentration losses take place, causing a progressive increase of the SOEC voltage (and correspondingly a decrease in the SOFC voltage). This leads to an increase of ΔV between the two components thus lowering the oxygen production efficiency.

2.2. System layout

In Fig. 6 the flowsheet of the integrated SOFC–SOEC device is shown. In this scheme, the SOEC anode side is fed (stream 8) with a H_2O rich stream coming from the SOFC anode. Inside the SOEC, oxygen is separated and sent to storage (stream 14). A multi-stage intercooled compressor is employed to bring the oxygen stream to ambient pressure when the SOEC anode operates at pressure lower than atmospheric. The stream at the SOEC anode side outlet (rich in H_2, point 7) is addressed to the SOFC anode for power generation. It should be noted that, due to the comparatively high operating temperature (about 750 °C), instead of a traditional blower an ejector ensures the recirculation of the H_2–H_2O mixture from the SOEC cathode outlet to the SOFC anode inlet. To this purpose, stream 9, a fraction of the stream at SOEC cathode exit, is sent to the heat exchanger where it is cooled down to a temperature (stream 10) acceptable for a compression carried out by a conventional blower. The heat exchanger also increases the system efficiency by preheating the air flow at the SOFC inlet (stream 3) with heat recovered from the streams of depleted air (stream 4) and oxygen (stream 12) exiting the SOFC and SOEC, respectively. The figure also shows the electricity and heat flow transferred from the SOFC to the SOEC. With reference to the latest aspect, the "sandwich" configuration proposed in Fig. 7 (obtained by overlapping layers of SOFC and SOEC realized according to a planar technology [11,12]) could be a solution to ensure an effective heat transfer between the components.

Moreover it is worth to note that for assigned values of cell active area and current density – being therefore fixed the O_2 yield – the solution with a high number of SOFC and SOEC cells of reduced area could be beneficial. In fact this determines: (i) a reduction of the current flowing across the stack which in turn brings about a

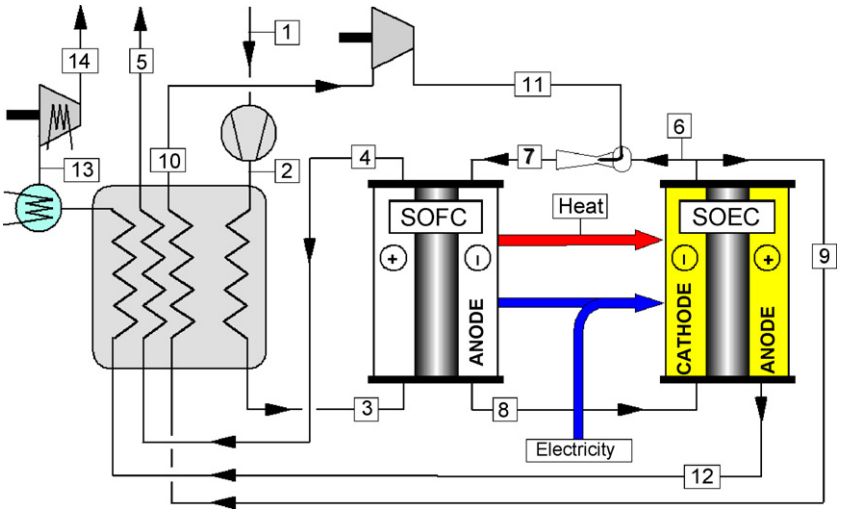

Fig. 6. Flowsheet of an integrated SOFC–SOEC system for pure oxygen production.

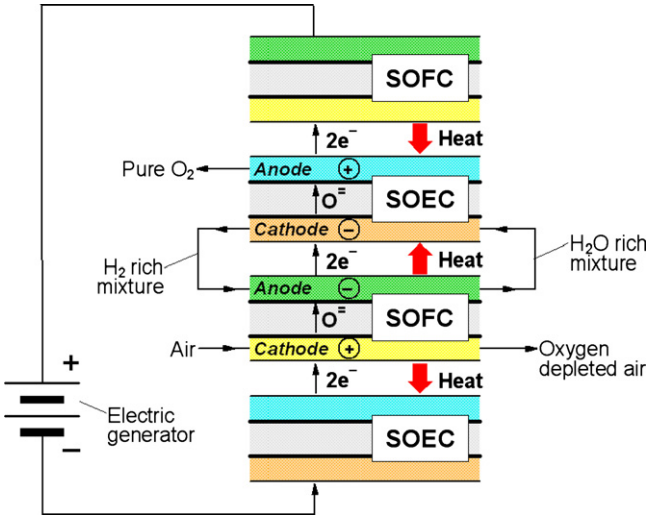

Fig. 7. Possible arrangement for assembling the SOFC and SOEC stack.

reduction of the ohmic losses – proportional to the square of the current[1] – in the circuit connecting the auxiliary electric generator with the SOFC–SOEC stack (Fig. 7); (ii) lower heat losses due to the lower value of the surface to volume ratio of the stack. In fact the thickness of a planar cell is typically much lower than the values of its length and width: therefore by assembling the stack with a higher number of small size cells it is possible to obtain a significant reduction of the area of the bottom and upper surface, with a comparatively small increase of the lateral stack surface. These considerations are reasonable within a certain number of cells in the stack as the benefit overcomes the disadvantages related to the increasing costs for interconnections and fluids distribution and to the reduced reliability.

As far as thermal balance is concerned, Fig. 7 shows that, owing to the endothermic and exothermic nature of the reactions within SOFC and SOEC, respectively, heat is transferred by conduction from the a SOFC cell to the two adjoining SOECs in the stack, while with regard to the electrical connections it can be noted that:

- SOFCs and SOECs are connected in series, meaning that, in steady state conditions, the current remains the same through the stack. (By definition the current flows in the opposite direction with respect to the electrons flow "$2e^{-}$" shown in Fig. 7.)
- Direct contact between the SOEC cathode and SOFC anode on one side, and between the SOFC cathode and the SOEC anode on the other side simplifies the electrical connection.
- Since in typical operating conditions the voltage delivered by the SOFC is lower than that required by the SOEC it is necessary to supply the required additional voltage, by means of an auxiliary generator; as already mentioned this component is responsible of the energy consumption of the device. Otherwise, the lack of potential can be compensated providing additional SOFC cell to the stack, which would be fed by a supplementary fuel source.

According to the previous indications, the proposed system shows the following advantages:

- The SOEC can dissociate the water molecules at high temperature and in vapour phase. Therefore it substantially reduces the electric absorption compared to the ordinary electrolyzers that operate at low temperature on liquid water.
- The SOFC generates electricity at very high conversion efficiency (50–70%). The remaining fuel input is released as high temperature heat available for SOEC (the vapour H_2O dissociation reaction is endothermic, the heat transferred from SOFC to SOEC allows to keep the system at the correct operating temperatures).
- The system does not consume any water.

3. Simulation model and results

To estimate the performance of the integrated SOFC–SOEC system depicted in Fig. 6, the main operating conditions and design parameters have been set and the complete energy balance has been calculated by means of a computer simulation. A 75% utilization factor[2] (for H_2 in the SOFC and H_2O in the SOEC respectively) has been assumed by setting the flow rate in the loop according to the generated O_2 flow rate.

The electric performance of the cells has been defined by means of the specific polarization curves shown in Fig. 5, where the voltage at open circuit ($I = 0$) is determined for SOFC and SOEC by Nernst equations (Eqs. (1) and (2)) assuming a mean value of 0.5 for the molar fraction of H_2 and H_2O. The complete polarization curves of SOEC are then obtained considering the cell overpotential as a function of the current density, taken from a simulation model developed for an IT-SOEC by Udagawa et al. [10]. In case of SOFC it is assumed that the basic components, materials and electrical properties and operating temperature are the same as SOEC and accordingly it is reasonable to consider that:

$$\frac{\partial V^{\mathrm{SOFC}}}{\partial I} = -\frac{\partial V^{\mathrm{SOEC}}}{\partial I}$$

meaning that, for a given current density I, the electrical losses which determines the change from the Nernst potential are the same for both SOFC and SOEC.

The pressure at which oxygen is separated within the SOEC is matter of optimization both from thermodynamic and technologic perspective. For an assigned final pressure of O_2 stream (14 in Fig. 7), in order to minimize the specific energy consumption it is necessary to minimize the sum of the power supplied by the auxiliary generator and the one required by the final compression which respectively increases and decreases with O_2 back pressure on the SOEC anode. Therefore, for a fixed value of current density in the stack, the optimized oxygen pressure depends on SOFC and SOEC[3] polarization curves and on the features of the final compression (namely number of intercooled stages and efficiency). According to the calculation assumptions reported in Table 1 the analysis shows that any pressure reduction has a beneficial effect on the system efficiency. A back pressure value of 0.1 bar has been selected as preliminary assumption to contain the number of compression stages and the volume flow rate on the SOEC anode side even if a complete design of the SOFC–SOEC device should include a mechanical stress analysis aiming to assess the electrolyte resistance to the pressure difference applied between anode and cathode. Under these assumptions, the resulting values of SOFC and SOEC Nernst potentials are 0.955 and 0.939 V, respectively.

Finally, the ejector's driving flow pressure and mass flow (stream 11) requested to overcome the pressure losses of the

[1] For a fixed value of the electric power, this implies a higher voltage provided by the auxiliary generator.

[2] The utilization factor is the ratio between the reacted moles of a species and the number of moles of that species at the component inlet.

[3] In principle, stream back pressure on the anode side may affect the SOEC polarization curve. This second order effect has not been considered in the present discussion.

Table 1
Simulation assumptions.

SOFC–SOEC current density ($A\,m^{-2}$)	500
SOFC operating voltage (V)	0.9179
SOEC operating voltage (V)	0.9760
Pressure losses in air piping (streams 2–5 in Fig. 6) (Pa)	2000
Pressure losses in H_2–H_2O loop (streams 6–8 in Fig. 6) (Pa)	400
Minimum ΔT within the recuperator (°C)	50
Cold blower:	
Isentropic efficiency	0.7
Organic/electric efficiency	0.8
Stream fraction to ejector driving flow	0.05
Ejector circuit compressor:	
Isentropic efficiency	0.7
Organic/electric efficiency	0.8
O_2 intercooled compressor:	
Number of stages	3
Intercooling exit temperature (°C)	35
Cooler pressure drop (Pa)	2000
Isentropic efficiency	0.75
Organic/electric efficiency	0.9

H_2–H_2O loop (streams 6–8 in Fig. 4) are calculated according to the analysis carried out in Appendix A.

Based on these assumptions, simulations of the system shown in Fig. 6 have been carried out with the ASPEN PLUS software. Properties of each streams in the relevant points of the flowsheet in Fig. 6 are reported in Table 2 while Table 3 reports the thermal balance summary. According to the above defined assumption set, for a current density of $500\,A\,m^{-2}$ the energy consumption is about 0.30 kW h per kg of generated O_2. It is worth to note that when the SOEC anode operates at atmospheric pressure, the energy consumption rises to 0.39 kW h $kg_{O_2}^{-1}$, a value comparable to the performance achievable by mid-size cryogenic air separation units, and significantly lower than the small scale units based on the PSA technology. Even higher efficiency can be achieved by adopting high temperature SOFC and SOEC that operate at about 1000 °C (the estimations here reported refer to intermediate temperature cells operating in the range 650–800 °C), or by assuming lower SOEC anode side back pressure.

On the other hand an increase of the current density brings about a higher O_2 flow rate but also a strong increase of the electric consumption due to the higher polarization losses and the reduced recuperator effectiveness. This can be seen from Fig. 8 where the difference between the SOEC and SOFC voltage profile (Fig. 8A) – which is the relevant parameter for the power consumption of the SOFC–SOEC system – and the specific consumption (Fig. 8B) are plotted as a function of the current density in case of O_2 back pressure on the SOEC anode of 1.01 bar and 0.1 bar, respectively. It

Table 3
Main results of the energy balance of the integrated SOFC–SOEC system.

Specific electric energy produced by the SOFC (kW h $kg_{O_2}^{-1}$)	3.075
Specific electric energy consumed by the SOEC (kW h $kg_{O_2}^{-1}$)	3.270
Specific electricity consumed by air blower (kW h $kg_{O_2}^{-1}$)	0.00928
Specific electricity consumed by the ejector circuit compressor (kW h $kg_{O_2}^{-1}$)	0.00860
Specific electricity consumed by the O_2 intercooled compressor (kW h $kg_{O_2}^{-1}$)	0.0885
Specific consumption (kW h kg^{-1} of pure O_2)	0.3010
Specific consumption (kW h Nm^{-3} of pure O_2)	0.4297
Heat exchanged between SOFC and SOEC (kW h $kg_{O_2}^{-1}$)	1.036
Heat exchanged within the recuperator (kW h $kg_{O_2}^{-1}$)	2.329

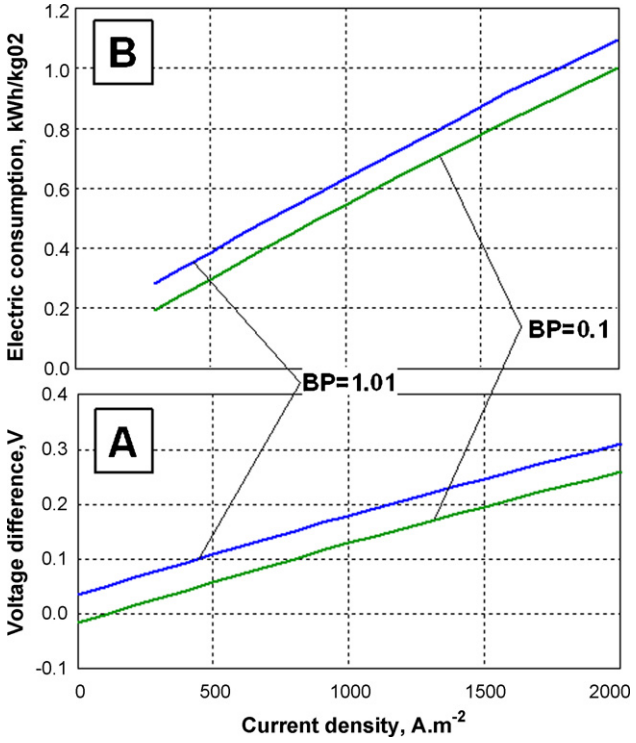

Fig. 8. Difference between the SOEC and SOFC voltage profile (A) and the specific consumption (B) plotted as a function of the current density in case of SOEC anode back pressure (BP) 0.1 bar and 1.01 bar.

Table 2
Properties of significant streams in the flowsheet shown in Fig. 6.

Point	°C	bar	kg $kg_{O_2}^{-1}$	kmol $kg_{O_2}^{-1}$	Ar	H_2	H_2O	N_2	O_2
1	15.0	1.013	11.50	0.3986	0.0100	0.0000	0.0100	0.7730	0.2070
2	17.3	1.033	11.50	0.3986	0.0100	0.0000	0.0100	0.7730	0.2070
3	700.0	1.028	11.50	0.3986	0.0100	0.0000	0.0100	0.7730	0.2070
4	750.0	1.018	10.50	0.3674	0.0109	0.0000	0.0109	0.8388	0.1395
5	79.7	1.013	10.50	0.3674	0.0109	0.0000	0.0109	0.8388	0.1395
6	750.0	1.013	0.5162	0.09896	0.0000	0.8000	0.2000	0.0000	0.0000
7	737.9	1.017	0.5433	0.1042	0.0000	0.8000	0.2000	0.0000	0.0000
8	750.0	1.015	1.543	0.1042	0.0000	0.2000	0.8000	0.0000	0.0000
9	750.0	1.013	0.02717	0.005209	0.0000	0.8000	0.2000	0.0000	0.0000
10	350.0	1.008	0.02717	0.005209	0.0000	0.8000	0.2000	0.0000	0.0000
11	503.2	1.823	0.02717	0.005209	0.0000	0.8000	0.2000	0.0000	0.0000
12	750.0	0.100	1.000	0.03125	0.0000	0.0000	0.0000	0.0000	1.0000
13	79.7	0.098	1.000	0.03125	0.0000	0.0000	0.0000	0.0000	1.0000
14	35.0	1.013	1.000	0.03125	0.0000	0.0000	0.0000	0.0000	1.0000

Mass and molar flow rates are referred to 1 kg of O_2 output. Compositions are given as mole percent of the total flow.

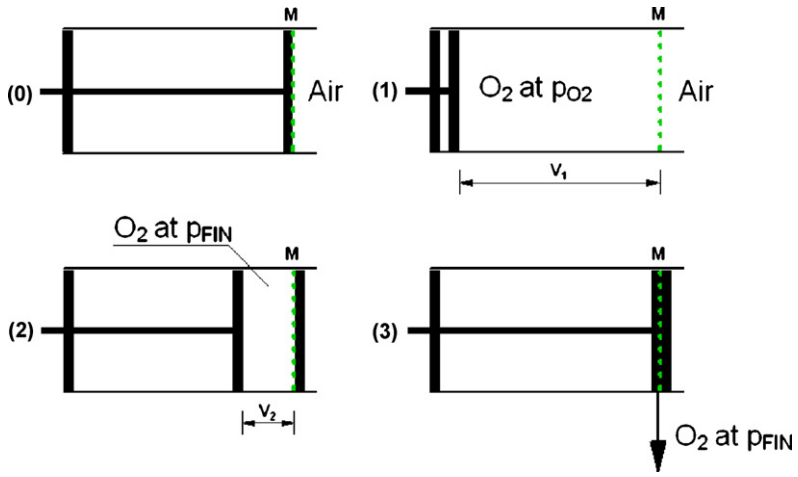

Fig. A.1. Conceptual schematics of an ideal, isothermal process to make available oxygen at pressure p_{FIN}, from ambient air.

can be seen that, assuming for instance a current density twice the base value (1000 vs. 500 A m^{-2}) and keeping the temperature of the cells at 750 °C by controlling the air flow rate on the SOFC cathode side, the oxygen production doubles, but the specific energy absorption substantially increases from 0.30 to 0.55 kW h kg^{-1} of pure O_2 for BP = 0.1 bar, and from 0.39 to 0.64 kW h $kg_{O_2}{}^{-1}$ for BP = 1.01 bar. However these results can still be acceptable if compared with low size oxygen production devices based on PSA technology.

As a final remark it is worth to emphasize that, being a typical modular system, this device allows to reach the desired O_2 product output by simply increasing the number of parallel modules without any performance decrease. Given that no significant scale effects can be predicted, small size appliances are expected to be the first commercial application of this technology (output in the range of 1–10 l min^{-1} of O_2 typical of home oxygen therapy treatments, or alternatively for O_2 production in hospitals). As far as the size of this appliance is concerned, a gross estimate of the bulkiest part of the system (the cell stack) can be done in case of small prototype with a 2.5 l of O_2 per minute yield. With a 1000 A m^{-2} current density and assuming a stack of 20 planar cells (10 operating as SOFC and 10 operating as SOEC), it results a block with a 720 cm^2 cross surface (approximately a 27 cm side square) and about 50 cm high, while a recuperator heat transfer surface of 0.063 m^2 can be estimated.[4] This would result fully comparable to commercial systems for small O_2 production used for home oxygen therapy treatments.

4. Conclusions

This paper described an integrated SOFC–SOEC device able to generate pure oxygen with an electric consumption comparable to mid-size cryogenic air separation units, and significantly lower than small scale systems based on the PSA technology.

This conclusion is the result of an investigation that accounted for the real operating conditions of the components. In particular, the performance of SOFC and SOEC at the design point has been assumed according to definite polarization curves of these components. The energy balance of the complete system, shows an electric specific consumption of about 0.30 kWh kg^{-1} of pure O_2 output when the system is operated at a current density of 500 A m^{-2}. Besides the clear advantages in term of energy and money savings, other favorable aspects can be envisaged over the competing technologies:

(1) The SOFC–SOEC technology virtually produces 100% pure oxygen. Such a result is not achievable in small-scale commercial system (typically based on PSA processes that allows to attain O_2 purity in the range 90–94%). For the large-scale system, the multiple columns configuration allows to achieve a purity close to 100% but it entails an increase of the energy consumption.
(2) Based on the fuel cell technology, the device is typical modular system. It is then possible to reach the desired O_2 product output by simply increasing the number of parallel modules without any performance decrease. Given that no significant scale effects can be predicted, small size appliances are expected to be the first commercial application of this technology (output in the range of 1–10 l min^{-1} of O_2 typical of home oxygen therapy treatments, or alternatively for O_2 production in hospitals), also considering that, in the case, a considerable energy saving would be achieved. From a preliminary design, the size of the device resulted fully comparable to commercial systems for small O_2 production used for home oxygen therapy treatments.
(3) It is also possible realizing a transportable appliance where the energy requirement is derived from liquid fuels (methanol or even gasoline) or provided by hydrogen stored in a bottle. With reference to the latest option and according to the results obtained, the device would be able to produce 1 Nm^3 of pure oxygen using 0.222 Nm^3 of H_2. Given that a bottle of pressurized gas can hold approximately the same amount (expressed in Nm^3) of gas, independently of it is filled with O_2 or H_2, the resulting benefit is the possibility to supply one bottle of H_2 instead of 4.5 bottles of O_2.

Appendix A. Calculation of the ideal work required for oxygen separation

The ideal work required to separate oxygen and made it available at pressure p_{FIN} in an isothermal process can be calculated considering the device shown in Fig. A.1(0): a piston sliding in a cylinder closed by an ideal membrane (M) perfectly permeable to O_2 but impermeable to the other air components. Initially the piston is at the top dead center in contact with the membrane. By moving leftward the piston (Fig. A.1), the volume in the cylinder increases and, since the membrane is in contact with air at atmospheric pressure, the volume is filled by the O_2 flowing through membrane at the partial pressure of O_2 in air (0.21 atm). The work produced by the piston in a reversible process is $L_1 = -p_{O_2} V_1$ (the negative sign means that work is applied by the fluid to the external environment) where V_1 is the volume swept by the piston in a complete stroke. When the piston reaches the bottom dead center, the cylinder is

[4] Calculated by assuming an overall heat transfer coefficient of 250 W m^2 K^{-1}, average value for a compact heat exchanger operating at ambient pressure.

closed with a lid that prevent the O_2 inside the cylinder to cross the membrane. Then the piston is moved rightward to compress the fluid to pressure p_{FIN} (Fig. A.1(2)).

By noting that the process is isothermal, compression work required in this phase can be computed as:

$$L_2 = -\int_{V_1}^{V_2} p\mathrm{d}V \tag{A.1}$$

Provided that the fluid behavior can be described by the ideal gas law, $pV = N_{O_2}RT$, the differential dV can be expressed as:

$$\mathrm{d}V = -\frac{N_{O_2}RT}{p^2}\mathrm{d}p \tag{A.2}$$

where N_{O_2} is the number of O_2 moles contained in the cylinder. By substituting (A.2) into Eq. (A.1) it follows:

$$L_2 = -\int_{V_1}^{V_2} p\mathrm{d}V = N_{O_2}RT\int_{p_{O_2}}^{p_{FIN}}\frac{\mathrm{d}p}{p} = N_{O_2}RT\ln\frac{p_{FIN}}{p_{O_2}} \tag{A.3}$$

In the last phase of the process, the pulsion work required to eject the O_2 from the cylinder is simply calculated as $L_3 = p_{FIN}V_2$. The overall work required is therefore $L = L_1 + L_2 + L_3$ but since the whole process is isothermal, $L_3 = -L_1$ and consequently $L = L_2$.

Finally specific consumption required in an ideal isothermal process that provides pure O_2 at p_{FIN} is given by the expression:

$$E_{rev} = \frac{L}{N_{O_2}} = RT\ln\frac{p_{FIN}}{p_{O_2}} \tag{A.4}$$

and coincides with the value obtained in Eq. (6).

Appendix B. Calculation of pressure losses and ejector model

As reported in Section 2.1, due to the high operating temperature (about 750 °C), the recirculation of the H_2–H_2O mixture from the SOEC cathode outlet to the SOFC anode inlet, is given by an ejector, instead of a traditional blower. A preliminary design of this apparatus can be made after calculation of the pressure losses within the SOFC–SOEC loop (streams 6–8) which determines the conditions of the ejector driving flow – in terms of flow fraction and pressure – necessary to provide the required ΔP.

Calculation of pressure losses is carried out as a function of the flow conditions within the SOFC and SOEC channels which are assumed to have a rectangular frontal size of 100 mm × 1 mm, according to [11]. Since the total mass flow of the H_2–H_2O mixture is fixed by the value of the desired O_2 yield, the pertinent mole flow value for each channel and the number of channels are calculated, given the density of the mixture (function of p and T, according to the ideal gas law), assuming an inlet velocity of 0.5 m s^{-1}. The length of each channels can consequently be obtained from the total cell active area which is calculated by the ratio between the current (which is also fixed by the desired O_2 yield), and the current density of the stack.

For the case considered in Table 1 with a current density of 500 A m^{-2} the active area is 24.1 m^2 (g_{O_2} s^{-1})$^{-1}$, resulting in 183 channels per g_{O_2} s^{-1} with length of 132 mm.

Once the channel length has been determined, pressure losses are finally calculated following a procedure already reported in [13] based on the fact that for laminar flow in a gas channel, the product of the skin-friction coefficient and the Reynolds number depends only on the channel dimensions [14]. For the case considered a pressure loss along the SOFC–SOEC piping of about 420 Pa has been obtained.

Given the pressure losses, it is possible to carry out a preliminary design of the ejector system. To this purpose an ejector model has been developed. With reference to Fig. B.1, the driving or primary

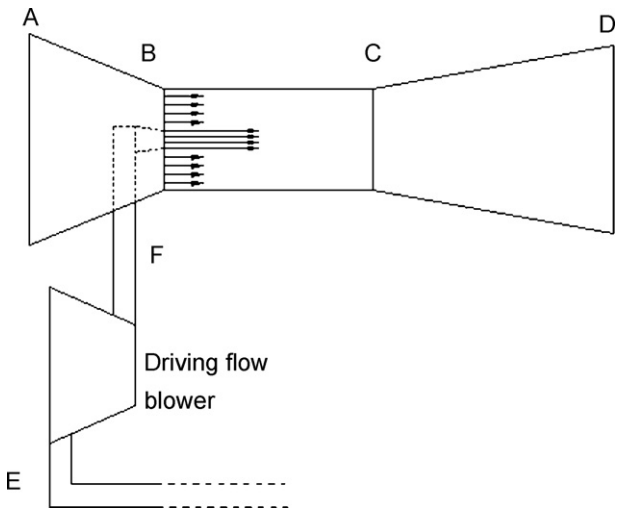

Fig. B.1. Schematic representation of the ejector.

flow at point E (representative of the conditions in terms of total variables of stream 10 in Fig. 6) is first compressed to an assigned pressure by means of a compressor with 0.7 isentropic efficiency. The flow is then expanded and accelerated in a convergent nozzle to the pressure of the secondary flow at section B. The secondary flow, whose conditions in terms of total T and p are those of stream 6 of Fig. 6, is expanded through a convergent from section A to throat B before being mixed with the driving flow. The two flows are then mixed (from section B to section C) and the resulting flow finally enters the diffuser section (from C to D) where kinetic energy is converted into pressure energy. A diffuser and convergent efficiency of 0.87 and 0.97, respectively are assumed in the calculation. These efficiencies are defined as follows:

$$\eta_{conv} = \frac{\Delta h_{re}}{\Delta h_{is}} \tag{B.1}$$

$$\eta_{diff} = \frac{\Delta h_{is}}{\Delta h_{re}} \tag{B.2}$$

where Δh_{re} is the variation of the static enthalpy along the actual transformation, while Δh_{is} is the variation of static enthalpy of an isentropic process reaching the same value of static pressure of the real case. The two terms Δh_{is} and Δh_{re}, are evidenced in Fig. B.2 in case of real and isentropic expansion (line AB and AB′, respectively)

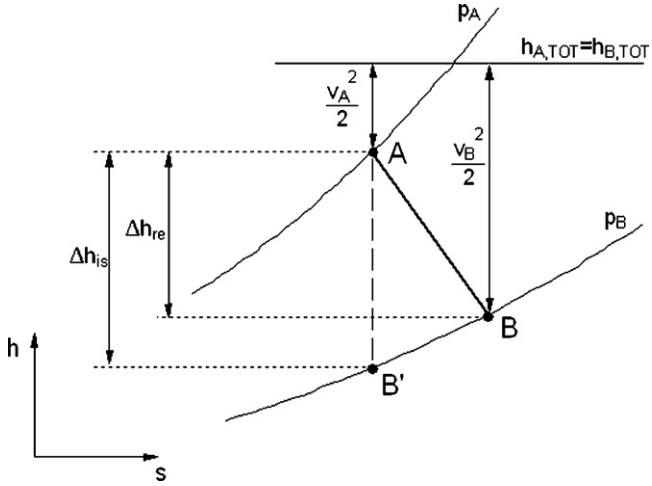

Fig. B.2. Expansion process through the convergent A and B (1). The variation of static enthalpy of the real process (Δh_{re}) and of the isentropic process (Δh_{is}) is evidenced.

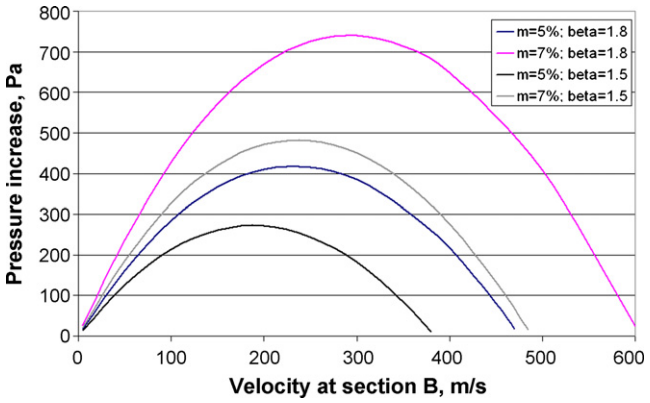

Fig. B.3. Results of the ejector model: pressure increase as a function of the velocity of the secondary flow for different sets of mass fraction and pressure of the driving flow.

through the convergent A and B of Fig. B.1. Analogous considerations can be made in case of the compression through the diffuser from C to D (Fig. B.2)

The model assumptions are:

- The flow is one-dimensional
- The mixing process occurs at constant pressure
- Wall shear stress are neglected in the throat (from section B to section C)
- Nozzle is adiabatic

The model input data are the following:

- mass fraction of the driving flow with respect to the total flow
- total temperature and total pressure of driving flow (section E) and secondary flow (section A)
- pressure ratio and efficiency of the driving flow blower
- convergent and diffuser efficiency defined according to Eqs. (B.1) and (B.2)
- velocity of the secondary flow at section B

The model applies mass, momentum and energy and conservation equations within the mixing section (B and C) allowing to determine for any input conditions the resulting pressure increase across the ejector (from section A to section D in Fig. B.1). Results of this analysis are reported in Fig. B.3 where the pressure increase is plotted as a function of the velocity of the secondary flow at section B (which is representative of the extent of the expansion of the secondary flow through A–B) for different sets of mass fraction and pressure of the driving flow.

As expected, the curves present a maximum given that, as the velocity of the secondary flow on section B increases, in the rising branch of the curve entropy losses related to mixing of streams at different velocity (from section B to section C) decrease faster than losses increase due to expansion (in primary and secondary flow nozzle) and diffusion (from C to D). It can also be noted that an optimized ejector can provide a 420 Pa pressure increase (the one required to overcame the pressure losses of the SOFC–SOEC loop) by adopting a driving flow mass fraction of 5% and a 1.8 pressure ratio. In this case the velocity of the secondary flow in the throat is about 230 m s^{-1} and the resulting geometry shows a proportion of the diameter of sections A:B:D equal to 1.0:0.15:1.02 with a overall length about seven times the inlet diameter.

References

[1] M.J. Kirschner, Oxygen, Ullmann's Encyclopedia of Industrial Chemistry, Wiley-VCH Verlag GmbH & Co. KGaA, 2000, doi:10.1002/14356007.a18_329.
[2] W.F. Castle, International Journal of Refrigeration 25 (2002) 158–172.
[3] A.R. Smith, J. Klosek, Fuel Processing Technology 70 (2001) 115–134.
[4] A. Sarofim, Proceedings of the 2nd Workshop of the oxy-fuel combustion network, Windsor (CT), USA, January 2007.
[5] Anon., Air Separation Process Technology and Supply System Optimization Overview, Universal Industrial Gases website, http://www.uigi.com/compair.html accessed on 9/9/08.
[6] R.M. Thorogood, in: B.A. Hands (Ed.), Cryogenic Engineering, Academic Press, London, 1986.
[7] O-Gen Industries Ltd., OG-200 and OG-475 Technical Data Sheets, www.ogenindustries.com accessed on 18 September, 2008.
[8] Air Products and Chemicals Inc., VSA Oxygen Generator – 40, 150 and 500 LPM Technical Data Sheets, www.airproducts.com accessed on 18 September, 2008.
[9] Technical Services, Inc., Science Applications International Corporation, Fuel Cell Handbook, U.S. Department of Energy Morgantown, West Virginia, 2004.
[10] J. Udagawa, P. Aguiar, N.P. Brandon, Journal of Power Sources 166 (2007) 127–136.
[11] P. Aguiar, C.S. Adjiman, N.P. Brandon, Journal of Power Sources 138 (2004) 120–136.
[12] S. Campanari, P. Iora, Fuel Cells: From Fundamentals to Systems 1 (2005) 34–51.
[13] P. Iora, P. Aguiar, C.S. Adjiman, N.P. Brandon, Chemical Engineering Science 60 (2005) 2963–2975.
[14] R.K. Shah, A.L. London, Laminar Flow Forced Convection in Ducts, Academic Press, New York, 1978.